

AEROSOL LIGHT ABSORPTION MEASUREMENT TECHNIQUES: ANALYSIS AND INTERCOMPARISONS

ANTONY D. CLARKE*, KEVIN J. NOONE†, JOST HEINTZENBERG‡, STEPHEN G. WARREN§
and DAVE S. COVERT†

*Hawaii Institute of Geophysics, University of Hawaii, Honolulu, HI, U.S.A. †Environmental Engineering and Science Program, University of Washington, Seattle, WA, U.S.A. ‡Department of Meteorology, University of Stockholm, Stockholm, Sweden and §Department of Atmospheric Sciences, University of Washington, Seattle, WA, U.S.A.

(First received 30 January 1986 and in final form 1 August 1986)

Abstract—A controlled study was carried out to evaluate three measurement techniques used for the determination of aerosol light absorption coefficients from aerosol samples collected on various filter substrates. These techniques were found to agree within about 10–30 % when applied to a range of filter loading obtained for a laboratory generated calibration aerosol. Microphysical properties of the calibration aerosol were used to model its optical effects using Mie theory. The measured and modeled optical properties were found to differ by less than 30 %. Qualitative and quantitative agreement of these techniques indicate that they provide a reasonable indirect method for the determination of atmospheric aerosol absorption coefficients and the related concentration of elemental carbon aerosol.

Key word index: Carbon, soot, aerosol, light absorption, optical properties.

INTRODUCTION

The optical properties of elemental carbon (EC) present in soot particles in the atmosphere are of interest in view of the potential effects that EC may have on radiative transfer in the atmosphere and on climate (Charlson and Pilat, 1969). These include effects in urban areas (Kawa and Pearson, 1984), regional effects of polluted air masses (Ball and Robinson, 1982), and the transport of this material in the troposphere such as pollution haze in the Arctic (Clarke, 1984; Heintzenberg, 1982) including its removal to the snowpack (Clarke and Noone, 1985). The interpretations of current effects and possible trends depend directly upon the ability to quantify the optical effects of aerosol EC concentration and its distribution in the atmosphere.

A variety of approaches for the measurement of EC are presently in use that often employ calibration methods, if any, that are particular to each technique. A summary of many of the current techniques can be found in the *Proceedings of the First International Workshop on Light Absorption by Aerosol Particles* (Gerber and Hindman, 1982) and in *Applied Optics*, Vol. 21, 1982. Here we present and intercompare results from three optical absorption techniques currently in use along with theoretical modeling of measured aerosol characteristics appropriate to the interpretation of optically derived data. Most attention will be given to the Integrating Plate (IP) method (Lin *et al.*, 1973; Weiss and Waggoner, 1982; Clarke, 1982a), Integrating Sphere (IS) method (Heintzenberg, 1982) and the Integrating Sandwich (ISW) method (Clarke, 1982b) using Monarch 71 (Cabot Corp.) soot

as a calibration aerosol. We will also report the results of incorporating a neutral density filter (NDF) in the standard IP method as a partial correction for possible overestimates of absorption by that method (Clarke, 1982a).

BACKGROUND

The presence of elevated concentrations of soot in the atmosphere associated with combustion sources is observed over many areas of the globe. This soot has EC as its major light-absorbing constituent which, when collected on appropriate substrates, causes a distinct discoloration (blackening or graying) of the filter. During the past two decades, increased interest and concern over the optical and climatic aspects of air pollution have led to the development of techniques that attempt to determine the important aerosol optical parameters [e.g. absorption coefficient, b_a and scattering coefficient, b_s , both with units of inverse length which together describe the single scatter albedo, $\tilde{\omega} = b_s/(b_s + b_a)$], needed for modeling atmospheric radiative transfer. These coefficients depend on the real and imaginary refractive indices of the particles and are also functions of the particle size distribution and the wavelength of light.

Numerous measurements of atmospheric aerosol have confirmed the bimodal character (accumulation mode and coarse mode) of the aerosol mass size distribution observed for particle diameters above 0.1 μm . In the atmosphere, most EC mass is confined to the accumulation mode and log-normally distributed with a geometric mass mean diameter, D_g , in the range of 0.1–0.5 μm with 0.2 μm as a representative value (Whitby, 1979). The value of D_g is influenced in

part by the nature of the sources, the fuel, type of combustion, dilution factors, residence time at different concentrations, and condensation processes on the particles. Although the integration of sources and dilution in urban areas tend to keep D_g at a few tenths of a μm , this variability can affect the overall optical characteristics such that any instrument calibration based on a certain size distribution may not be appropriate for a measured atmospheric aerosol having a different size distribution.

Except under unusual circumstances associated with very high concentrations of crustal dust (the only common natural non-combustion-derived absorber) in the atmosphere, b_a is dominated by absorption due to EC (Heintzenberg, 1982; Weiss and Waggoner, 1982). This is due to the large value of the imaginary part of its complex refractive index (Jantzen, 1979; Twitty and Weinman, 1971) which is about one to two orders of magnitude greater than natural crustal absorbers at 550 nm wavelength. This results in a large value for the mass absorption coefficient, B_a (units m^2g^{-1} , also called specific absorption), for EC (Roesler and Faxvog, 1980). B_a is a property of the individual particles; it must be multiplied by the mass concentration of particles in the atmosphere to obtain b_a .

Measurement of aerosol light-absorption coefficients are directly valuable for studies of atmospheric visibility, radiative transfer, and atmospheric heating rates, while determinations of EC concentrations are of direct value for source monitoring and for the study of life cycles of EC aerosol. In principle, it should be possible to convert either type of measurement into the other by using appropriate values for specific absorption, B_a . While this conversion is routinely done in the reporting of data collected using some of the techniques currently in use, these reports frequently overlook details of the assumptions made and the consequent uncertainties inherent to this type of conversion. Apart from instrumental calibrations and measurement uncertainties, a given mass of EC aerosol can yield significantly different optical properties (e.g. B_a , ω) depending upon such things as the geometric mass mean diameter, D_g , and shape of the size distribution, the morphology of the particles, the complex refractive index, and the presence of particle coatings or condensates. Since EC size distributions are seldom measured coincidentally with either light absorption or total EC mass concentration, this uncertainty in the conversion factor should be kept in mind when conversions are made between EC concentrations and associated optical effects. Some of these considerations, both observed and modeled theoretically, will be presented here as they relate to our calibrations and intercomparisons.

EXPERIMENTAL

Figure 1 is a flow diagram of the experimental apparatus used to generate and sample EC aerosol. Heintzenberg (1982)

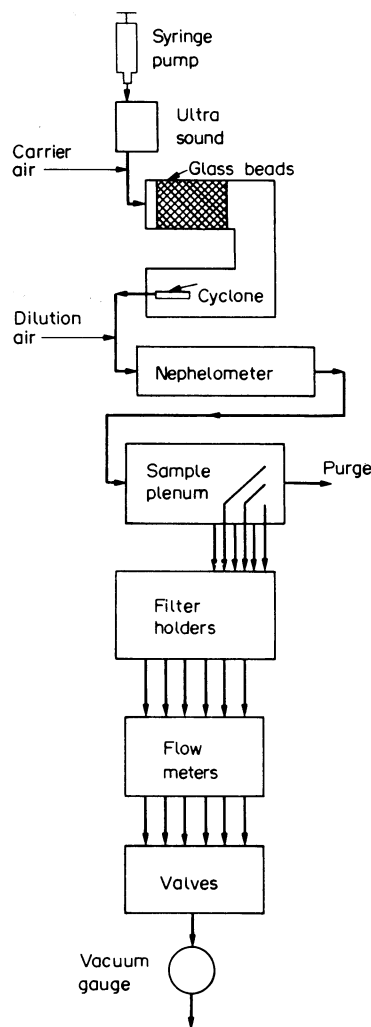


Fig. 1. Schematic diagram for aerosol generation and sampling system used for M71 test aerosol (see text).

introduced the commercially available channel soot Monarch 71 (M71) as a reference material for absorption of light by aerosol. For this comparison, a hydrosol prepared from 100 mg of M71 was mixed in 80 ml water with 20 ml isopropyl alcohol added to improve soot miscibility before being placed in an ultrasonic water bath for 30 min to disperse the M71 particles. The hydrosol was then put into a Harvard syringe pump and injected continuously into a filtered carrier air stream via a 1 mm-diameter catheter tube submerged in an ultrasound bath to prevent coagulation and deposition to the walls of the tube. The suspension was nebulized to form an aerosol, diluted with dry filtered air, dispersed through a bed of glass beads and drawn through a modified cyclone (Bendix-Model 18) to remove most particles greater than $0.8\ \mu\text{m}$ diameter. The aerosol stream was then diluted a second time with dry filtered air before entering an integrating nephelometer (Meteorology Research, Inc. 1550, $\lambda = 490$) used to measure the scattering coefficient of the aerosol. The size distribution of the M71 test aerosol generated here (mass mean diameter = $0.59\ \mu\text{m}$, $\sigma_g = 1.47$) resulted in only a 1% difference in the calculated mass scattering coefficient for $\lambda = 490\ \text{nm}$ and $\lambda = 550\ \text{nm}$. Hence, comparison of b_s values to b_a measured at $\lambda = 550\ \text{nm}$ is possible without corrections for this particular size distribution. After passing through the

nephelometer, the air stream went to a vertical plenum tube. Six sampling ports and filters were arranged to ensure identical sampling of the aerosol stream. Valves controlled flows which were measured using calibrated dry gas meters and set so that M71 mass loading per unit area on each filter would be similar. A calibration of each gas-flow meter referenced to a wet test meter was carried out prior to the experiment, and flow corrections for each meter were determined. After correction, the resultant flow uncertainty is about 3% or less. Measurements of effective filter areas are prone to a systematic uncertainty of about 4%. The resulting absolute uncertainty in sampled air volumes, except for very low flows, is considered to be less than 8%. One filter from each test, hereafter called mass filter (25 mm diameter, 0.4 μm pore size Nuclepore), was operated at high flow rate in order to collect a mass of EC sufficient for gravimetric analysis and weighed three times on a CAHN electrobalance before and after exposure. This measured mass and the volumes sampled were used to estimate mass on the remaining filters used in the optical calibration, all of which had too little deposited soot to allow gravimetric determination. This arrangement also allowed the mass filter, having optical absorbance of 10–40% for the IP method, to be compared to the order-of-magnitude lower mass per unit area on the other filters analyzed by the more sensitive IS and ISW methods. The results reported here will refer only to measurements on Nuclepore (0.4 μm pore diameter) and Microsorban latex (Delbag A. G., Berlin) as these are most commonly used for the methods being compared here.

ABSORPTION MEASUREMENT METHODS

The integrating plate method (Lin *et al.*, 1973) has been used by numerous investigators due to its simplicity. A light-diffusing support (e.g. opal glass), Fig. 2a, is used to provide a nearly Lambertian light source upon which a substrate (typically 0.4 μm Nuclepore filters) can be placed for analysis. The transmission of the substrate is measured before and after the collection of aerosol particles, and the change in transmission is related to the absorbing component of the aerosol. As originally presented it was argued that, because the light striking the substrate was isotropic in one hemisphere, the amount of light in the transmitted flux scattered away from the detector was equal to that scattered toward the detector, so that the net transmission change was due to the absorption only. It was recognized that light backscattered from the aerosol was not directly accounted for in this arrangement but this was not considered a substantial error due to the typically small fraction of light scattered into the backward direction by most ambient aerosol. Consequently, the IP method was considered to yield aerosol optical depths directly from the measured transmission change on the filter by application of Beer's law, $I/I_0 = \exp(-d)$ (where I_0 is initial intensity, I is final intensity and d is the optical depth). The original description and tests of the IP claimed accuracy only to within a factor of two, but a subsequent field test (Weiss and Waggoner, 1982) showed agreement with other independent techniques within about 25%.

Numerous IP measurements of laboratory and ambient aerosol later revealed that a systematic overestimate of the absorption of light by fine particles

appeared possible with this method. These observations indicated that the presence of aerosol on the Nuclepore surface could alter the internal reflection coefficient of the filter in a way that results in increased absorption of the particle/filter combination. This effect and measurements of the back reflectance changes of the filters that can be introduced in an optical model to obtain the corrected absorption are discussed elsewhere (Clarke, 1982a). While the exact effect depends on a variety of factors and decreases with higher concentrations of absorbers on the filter, a 30% positive bias of absorption for typically measured transmission changes (about 10–30%) is not uncommon. This has recently been confirmed independently by more direct methods (Weiss and Waggoner, 1984). A method that provides a partial reduction of this bias, achieved simply by placing an appropriate neutral density filter (NDF) between the Lambertian reflector and the substrate (Clarke, 1982a; illustrated in Fig. 2b), is included as one of the measurement types reported here.

A third and more sensitive technique, the integrating sandwich (ISW), has been developed for very low concentrations of absorbing material present on a substrate. Here the substrate is placed between two plates, each with diffuse reflectance of about 96% (Fig. 2c). Light penetrating one side of the 'sandwich' experiences multiple diffuse reflections inside the sandwich while passing through the substrate and thereby amplifies the net absorption by the aerosol as determined by a detector on the other side of the 'sandwich.' Optical properties of the Nuclepore filter substrate are included in the modeled response to the instrument, and results agree well with the laboratory calibration of the ISW. Though nonlinear, the response provides a gain in sensitivity of about 40 for filter transmission changes less than a few% and allows rapid sample collection for low ambient levels of absorbing aerosol. Measurements are insensitive to the relative amounts of scattering aerosol present and (like the IP and IP-NDF methods) are non-destructive to the samples. Both theory and instrument calibration are presented elsewhere (Clarke, 1982b).

The integrating sphere (IS) technique for measurement of light absorption by aerosol was described by Fischer (1970). It was modified in the present instrument to increase the precision of the optical measurement while accommodating samples collected on various substrates. A sphere, its inside coated with diffusely reflecting white paint, is illuminated through a small hole (Fig. 2d). The light (550 nm wavelength) strikes the absorption sample suspended in the center of the sphere. Part of the light is absorbed by the sample and the remainder is transmitted by the sample or reflected to the walls. The detector, which is screened from direct light, measures the light reflected from the walls through another hole in the sphere. This arrangement ensures that any reduction in signal after insertion of a sample will be due to absorption by the aerosol particles. The detected signal is referenced to

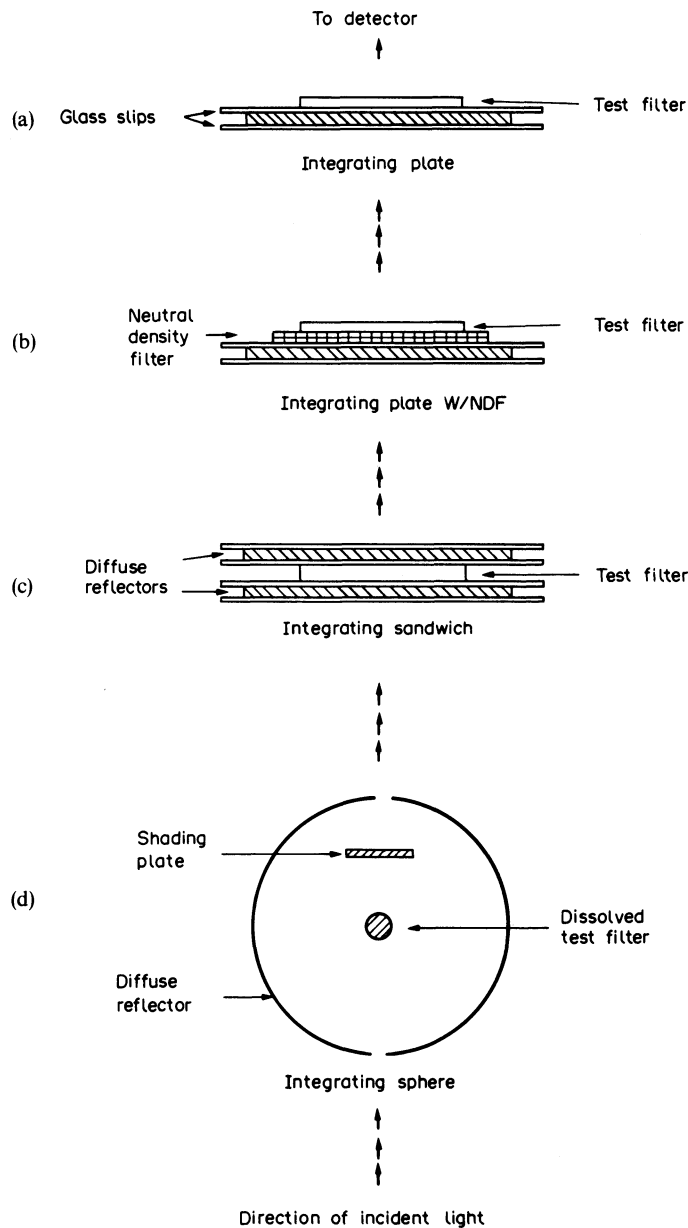


Fig. 2. Schematic illustration of principal features of the four indicated measurement methods being compared here. Each method is shown with incident light approaching from below and being detected above after passage through the system: (a) Integrating Plate (IP); (b) Integrating Plate with neutral density filter (IP-NDF); (c) Integrating Sandwich (ISW); (d) Integrating Sphere (IS).

light leading from the incandescent lamp, through a chopper, to the detector. A microcomputer measures the light signals consisting of photon counts from a photomultiplier tube while sensing the position of the chopper blade. The all-digital operation of the photometer allows high precision measurements down to about 0.1 % transmission change due to the sample. A sample consists of aerosol material deposited on polycarbonate film or latex fibres (Microsorban) which have been dissolved in 3.5 ml dimethylchloride and

dispersed in an ultrasound bath. It rests in a round glass flask suspended on a glass bar. As sample treatment is destructive, it comes last in any sequence of chemical analyses. However, it has several advantages:

- (1) The particles are suspended in a solution during the optical analysis, which is closer to their airborne state than measurements on thick deposits, and closer to conditions assumed in Mie scattering calculations.
- (2) Interfering effects by non-absorbing (but scat-

tering) particles in the sample are reduced by raising the refractive index of the suspending medium from 1.0 (air) to 1.35 in the solution.

(3) Samples can be analyzed in parts to avoid nonlinear responses at the high end of the absorption scale (Heintzenberg, 1982).

(4) The optical effects of light-absorbing organics in the sample is reduced by dissolving the sample in dimethyl chloride (Heintzenberg, 1982) (this could possibly result in improved EC estimates but less accurate atmospheric absorption coefficients).

Primary IS calibration is based on absorption measurements made on samples of our reference soot M71 which have been weighed on a microbalance and then volume-diluted to achieve optical signals covering the whole working range of the instrument (0.1–100 μg of M71 per sample). IS measurements are reported either in terms of optical equivalent weights of M71 or absorption coefficients based upon the specific absorption of $9.68 \text{ m}^2 \text{ g}^{-1}$ (Donoian and Medalia, 1967) determined for M71 aerosol when particle diameters above $0.45 \mu\text{m}$ diameter are excluded. More details about the instrument are given by Heintzenberg (1982).

This paper will present and intercompare data from the above techniques: IP, IP-NDF, ISW, IS and for either the same filter sample or filter samples collected in parallel during the experiment. In addition, some reference to other data will be made when appropriate.

RESULTS

In order to judge the relative constancy of the aerosol optical properties at the various concentrations used during the test, we plot b_a obtained from the Nuclepore filter on which the primary measurement was made against b_s (Fig. 3) for all samples. The values for b_s were obtained directly from the nephelometer which had Rayleigh scatter removed but have been multiplied by 1.1 to adjust for an estimated 10% angular truncation error in this instrument for particle sizes used here (Weiss and Waggoner, 1984). The values for b_a were determined using the IP method with corrections based upon the change in back reflectance from the filter as a function of transmission change (Clarke, 1982a). For the range of b_a measured here these corrections resulted in a 10–25% reduction from values using the uncorrected IP method. Error bars in Fig. 3 represent our assessment of uncertainties in instrument precision for measurements of both b_a and b_s . The slope of the fitted line corresponds to a mean single-scatter albedo of about 0.40, a property of the aerosol that does not depend on concentration. The constancy of this ratio also indicates that the aerosol optical properties and size distribution of the M71 did not change significantly during the experiment, as was supported by a sample of scanning electro-micrographs (SEM) of these filters, so that comparisons of data from different samples are valid.

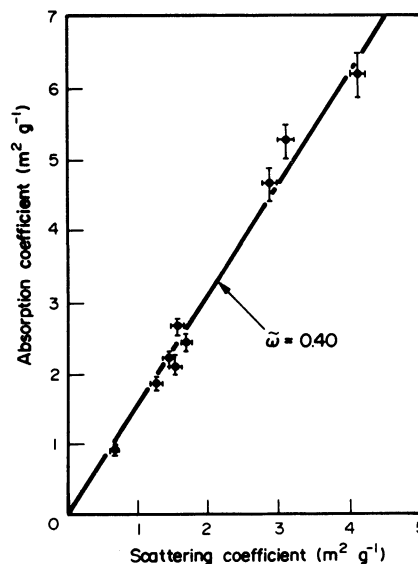


Fig. 3. Experimental plot of the absorption coefficient vs scattering coefficient for all aerosol concentrations used for the M71 test aerosol generated as per Fig. 1. A visual best fit line through the data has the indicated single scatter albedo of 0.40.

A direct comparison of three sets of data are presented in Fig. 4 for the IS using Microsorban and Nuclepore filters and the ISW using the Nuclepore filter. Each point is plotted as the estimated particle mass based on the gravimetric mass measurement and

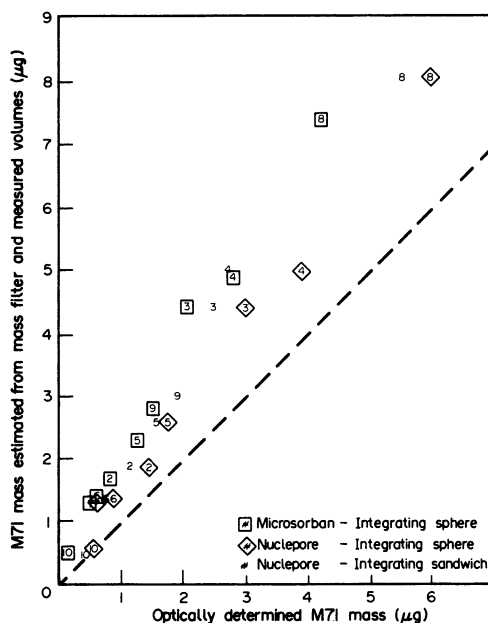


Fig. 4. Plot of estimated filter M71 mass based on filtered volumes relative to weighed test filter vs the M71 mass inferred from optical measurements using the three indicated techniques and an assumed specific absorption, B_a , of $9.68 \text{ m}^2 \text{ g}^{-1}$ (see text).

Table 1. Intercomparison test data

Sample	Mass NUC. (μg)	Mass UNCER. (%)	B_a	B_a	B_a	B_a	B_a	B_a	B_a	B_a	B_a	B_a	B_a
			IP M.F. ($\text{m}^2 \text{g}^{-1}$)	NDF M.F. ($\text{m}^2 \text{g}^{-1}$)	M.F. ($\text{m}^2 \text{g}^{-1}$)	IP* M.F. ($\text{m}^2 \text{g}^{-1}$)	ISW NUC. ($\text{m}^2 \text{g}^{-1}$)	IS NUC. ($\text{m}^2 \text{g}^{-1}$)	ISMICR. ($\text{m}^2 \text{g}^{-1}$)	ISMICR/ IS NUC.	ISMICR/ ISW NUC.		
M71-1	6.50	15.36	6.78	6.08	4.73	4.89	7.27	4.55	0.63	0.93			
M71-2	15.10	6.62	6.94	6.04	4.71	5.53	6.60	4.65	0.70	0.84			
M71-3	24.00	4.17	7.49	5.07	4.78	6.36	6.99	5.49	0.79	0.86			
M71-4	8.40	11.90	6.69	5.65	4.66	5.36	6.32	5.09	0.81	0.95			
M71-5?	4.60	21.74	7.52	6.03	5.37	4.66	5.80	4.24	0.73	0.91			
M71-6?	4.50	22.22	5.23	4.14	3.71	3.79	4.45	3.67	0.82	0.97			
M71-7	26.10	3.83	6.97	6.51	4.50	6.39	7.05	5.44	0.77	0.85			
M71-9	14.50	6.90	7.91	7.57	5.32	5.71	8.09	5.08	0.63	0.89			
M71-10?	2.60	38.46	9.80	11.11	7.00	6.88	10.87	2.70	0.25	0.39			
Mean	[5,6,10 excluded]		7.13	6.15	4.78	5.70	7.05	5.06	0.72	0.88			
Std. dev.	[5,6,10 excluded]		0.47	0.84	0.23	0.59	0.61	0.39	0.08	0.05			
UW AMBI1	31.80		1.09	0.97	0.71	0.59	0.46	0.37	0.80	0.62			
UW AMBI2	61.00		1.34	1.16	0.94	0.93	0.87	0.69	0.79	0.74			
M71WEISS1	25.00		8.90	8.25	7.30	(7.5)	—	—	—	—			
M71WEISS2	24.00		9.67	8.96	8.00	(8.5)	6.90	—	—	—			

* = IP data corrected from back reflectance measurements (Clarke, 1982a).

() Measured with extinction cell (Weiss and Waggoner, 1984).

? = Mass uncertain due to low measured mass on filter.

Abbreviations: NUC = Nucleopore; UNCER = percent mass uncertainty; ISW = Integrating Sandwich; IS = Integrating Sphere; IP = Integrating Plate; NDF = Neutral Density Filter; MICR = Microsorb; Std. dev. = Standard deviation of mean quantities.

relative sample volumes vs the optically estimated mass based upon an assumed specific absorption, B_a of $9.68 \text{ m}^2 \text{ g}^{-1}$ for all methods. The dashed line represents perfect agreement between measured and optically determined masses. Several observations can be made from the figure:

(1) All methods show relatively good agreement and linear responses over an order of magnitude change in M71 mass. The IS (Nuclepore) method appears to give systematically higher and more variable absorption estimates than the other two.

(2) The IS (Microsorban) and ISW (Nuclepore) measurements agree quite well and often differ by less than that due to the 8 % uncertainty in flow rate.

(3) All methods indicate less absorption for a given measured M71 mass than expected. This is a consequence of the properties of the size distribution of the test aerosol resulting in a lower value of B_a than $9.68 \text{ m}^2 \text{ g}^{-1}$ and is not due to instrumental calibration, as shown below.

(4) The overall differences between these methods appear to be less than the variability expected in atmospheric EC optical properties, as shown below.

The IP and ISW methods have the advantage of determining an absorption coefficient independent of mass on the filters. However, intercomparison with the IS measurements and the modeled properties of the size distribution is facilitated by making comparisons of the specific absorption, B_a , obtained by each technique. The IS technique uses measured absorption to make a determination of soot mass based upon a measured value of $B_a = 9.68 \text{ m}^2 \text{ g}^{-1}$ (Donian and Medalia, 1967) for M71 particles with diameters below 0.45 μm . Hence, the ratio of the M71 mass inferred from IS measurements to the measured M71 mass on the test filter can be multiplied by this value of B_a to obtain the effective B_a for these samples using IS technique. This value can then be compared to the B_a values determined by the IP and ISW methods, as shown in Table 1 for the same data plotted in Fig. 4.

M71 masses and the % uncertainty for each of the ten runs are included in columns 2 and 3 of Table 1. The remaining data are presented as the specific absorption values determined from measured masses and the absorption determined from each technique. Columns 4, 5 and 6 are, respectively, the integrating plate measurements on the mass filter for the uncorrected IP method, neutral density filter IP-NDF, and model-corrected IP values after Clarke (1982a). Column 7 is the ISW value for the Nuclepore filter including the model filter corrections. Columns 8 and 9 are IS data for Nuclepore and Microsorban filter data, respectively. Column 10 is the ratio of IS Nuclepore to IS Microsorban B_a values and 11 is the ratio of IS Microsorban to ISW Nuclepore B_a values. In calculating the means and standard deviations given in Table 1, samples numbered 5, 6 and 10 were ignored because of mass uncertainties greater than 20 % due to the low mass on the filters. The ambient samples in Table 1 will be discussed later. In spite of a limited data

set, the following observations can be stated:

(1) The Integrating Plate (IP) data show a decrease in apparent absorption for the neutral density filter (NDF) measurement and a further decrease for the values corrected by the model of Clarke, 1982.

(2) Integrating Sandwich (ISW) modeled values lie between the IP-NDF and IP model values.

(3) Integrating Sphere (IS) samples collected on Nuclepore filters are higher than those on Microsorban filters by about 40 %, significantly greater than that due to a maximum possible systematic uncertainty (about 15 %) in the ratio of their flow rates.

(4) Integrating Sphere Microsorban values are about 12 % lower than Integrating Sandwich Nuclepore values and remain within the maximum systematic uncertainty of 15 % in their ratio.

(5) Most values of B_a are considerably lower than the $9.68 \text{ m}^2 \text{ g}^{-1}$ obtained by Donian and Medalia for M71 particles with diameters less than 0.45 μm .

In order to compare the above results to those from another approach, we also examined two samples (M71WEISS1 and M71WEISS2) generated from a sonic jet in a M71 suspension followed by an impinger for the removal of larger particles (Weiss and Waggoner, 1984). These were measured using the three IP methods indicated in Table 1. The two values for B_a in parentheses for these samples are those directly measured with the extinction cell (Weiss and Waggoner, 1984). Values of B_a are significantly higher for each method than the values of the M71 prepared for the test described above. This difference can be accounted for by observed differences in the M71 aerosol size distribution (Figs 5 and 6). A third test, Table 2, compared filtered hydrosol samples prepared from a weighed mass of M71 (Heintzenberg, 1982) that was diluted to three different concentrations. Three filtrations of each dilution were made; two were measured using the Integrating Sandwich and one was measured using the Integrating Sphere. The ISW determinations were in close agreement with the expected value based upon the dilution. The IS values (Table 2) showed changes consistent with the dilutions but were about 25 % lower than ISW measurements and the expected values.

Table 2. Hydrosol test

Hydrosol	Expected mass μg	ISW NUC. mass μg	IS NUC. mass μg	IS MICR/ ISW NUC.
M71 201	0.57	0.50		
M71 202	0.57	0.53		
M71 203	0.57	—	0.46	0.89
M71 101	1.90	1.94		
M71 102	1.90	2.04		
M71 103	1.90	—	1.32	0.66
M71 301	5.70	5.82		
M71 302	5.70	6.23		
M71 303	5.70	—	4.14	0.69

See Table 1 for abbreviations.

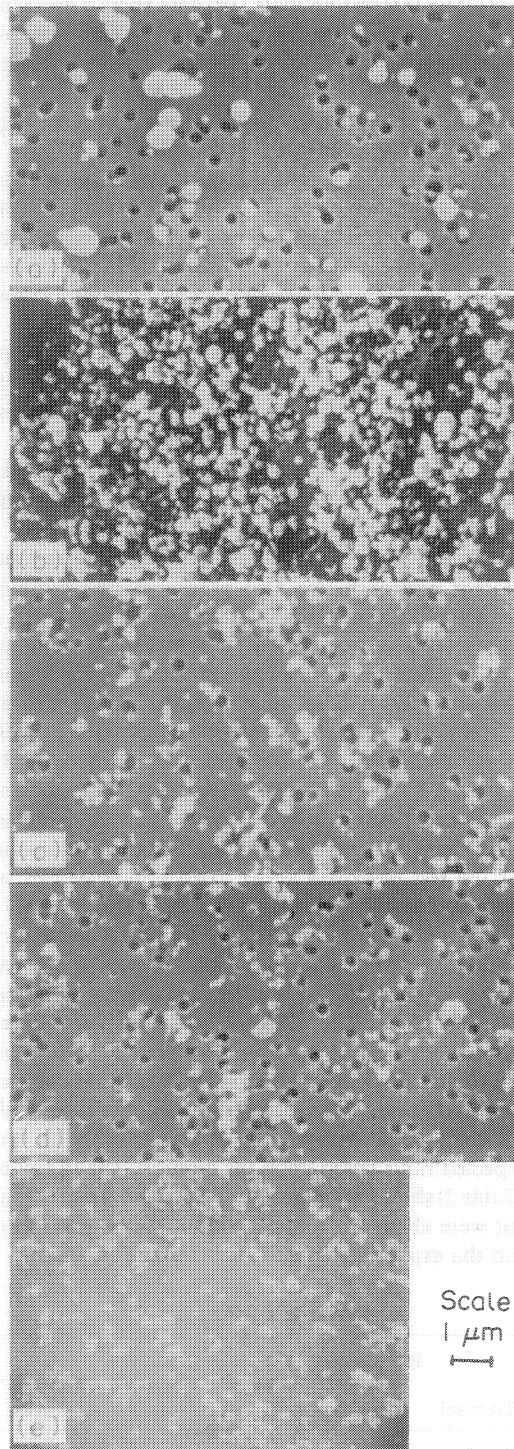


Fig. 5. Scanning Electron Micrographs for several aerosol samples discussed in the text. Associated mass mean diameters and geometric standard deviations in μm are: (a) M71 test aerosol, $D_p = 0.57$, $\sigma_g = 1.47$; (b) M71 Weiss, $D_p = 0.40$, $\sigma_g = 1.39$; (c) ambient tunnel, $D_p = 0.24$, $\sigma_g = 1.30$; (d) ambient UW (University of Washington), $D_p = 0.27$, $\sigma_g = 1.30$; (e) M71 hydrosol, $D_p = 0.31$, $\sigma_g = 1.36$.

Two samples of ambient aerosol collected at the University of Washington campus and a motor vehicle tunnel in central Seattle were also taken for inter-comparison purposes. Soot is only a small fraction of the total filterable mass in most urban atmospheres, so the specific absorption values are understandably much smaller for ambient samples compared to those of M71 (see Table 1). The overall relationships between the various measurement techniques on ambient samples are similar to those mentioned for the M71 inter-comparison. However, the ratio of absorption for IS Microsorban to ISW Nuclepore is about 0.7 compared to the 0.88 average for M71. More inter-comparisons of ambient aerosol must be done before this difference can be interpreted.

THEORETICAL ANALYSIS

The optical properties of a specific aerosol depend upon its size distribution. Here we present the aerosol size distributions measured for the above experiment in order to compare theoretical and measured aerosol optical properties. Figure 5 shows five scanning electron micrograph (SEM) photos for some of the aerosol samples discussed here. Manual sorting was performed on enlarged SEM photos in order to generate representative size distributions for each. Approximately 20 size bins for particle diameters between 0.06 and 0.90 μm were used to partition the aerosol. The resulting distributions were plotted on log-probability paper and found to be essentially log-normal. Log-normal 'best fits' to the mass distributions were performed by computer and the fitted parameters describing the distributions are included in the caption of Fig. 5. 'Best fit' parameters were considered valid when differences between calculated values for specific absorption and specific scattering determined for the measured size distributions and the parameterized log-normal distributions were less than a few %. Differences between optical properties determined for the measured size distributions and the log-normal 'best-fit' distributions were not significant, even though the shapes of the measured distributions differ greatly from the log-normal shape (compare Fig. 6a with 6d). This indicates that at most only two parameters (D_p , σ_g) are needed to characterize a distribution for the purpose of absorption and scattering by a polydispersion of soot particles.

Mie theory describes the interaction of an electromagnetic wave with a homogeneous sphere. The theory is applicable to soot spheres if their compositional inhomogeneities occur only on spatial scales smaller than the wavelength, which is probably true in most cases for soot. The soot particles are not spheres, and the method to be used for estimating the radius r of an 'equivalent' sphere (with the same absorption and scattering cross-sections) depends on the wavelength λ . For particles with $r \ll \lambda$ the equal-volume sphere is appropriate, whereas for $r \gg \lambda$ the sphere with the

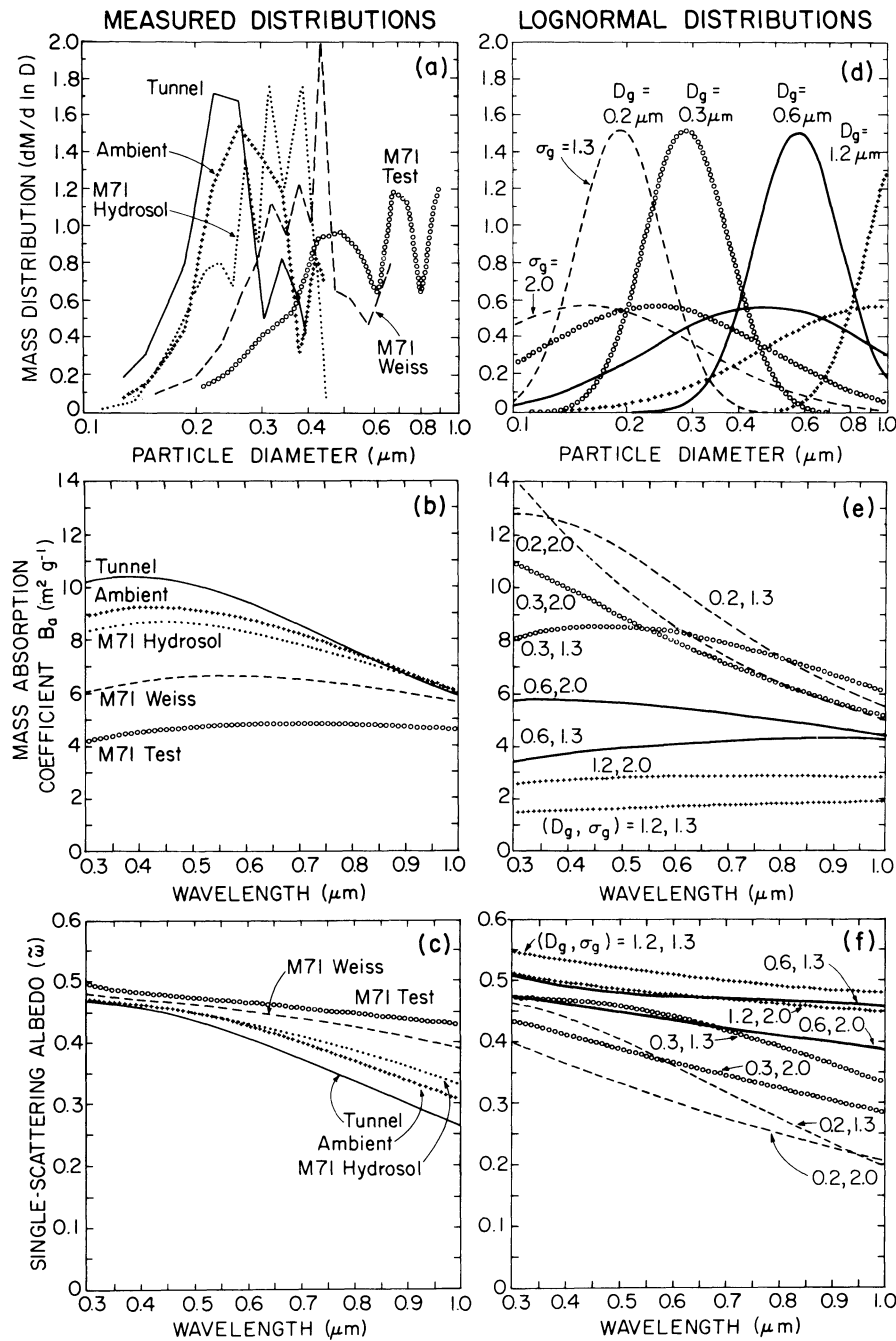


Fig. 6. Optical properties of soot, calculated using Mie theory, for measured and lognormal size distributions. The measured size distributions shown in (a) were obtained for the micrographs shown in Fig. 5. The last two points on the 'M71 test' size distribution are very uncertain due to the small number of particles in these large size classes. The lognormal distributions are characterized by their mass mean diameters D_g and their lognormal widths σ_g . The lognormal fits corresponding to the measured size distributions are given in Fig. 5. The B_a and ω from those lognormal fits agree well with those calculated from the measured size distributions.

same surface/volume ratio is the best equivalent sphere. [In the latter case the number of equivalent spheres per unit volume is different from the number of true nonspherical particles, so that both the total surface area and the total volume are conserved in going to the equivalent-sphere description.] This latter

formula for finding equivalent spheres was found by Pollack and Cuzzi (1980) also to be valid for particles of size comparable to the wavelength, which is the case of interest in this paper, for the purpose of calculating scattering and absorption cross-sections. The scattering theory for spheres is used here in Fig. 6 simply

because it is what is available. The scattering by nonspherical particles can differ greatly in the details of the phase function, especially for very nonspherical particles. The particles shown in the electron micrographs in Fig. 5, however, are roughly equidimensional so that the use of scattering theory for spheres is probably not a large source of error, especially since we are computing only angular-averaged quantities, not the phase functions. The Mie calculations use the algorithms of Wiscombe (1980), and they all use complex refractive index $m = 2.00 - 0.66i$. This was recommended by Bergstrom (1972, 1973) based upon measurements of Senftleben and Benedict (1917). It is used here as a typical value, but different types of soot will of course have somewhat different values of m . For example, Jantzen (1979) obtained $m = 2.0 - 1.0i$, whereas Roessler and Faxvog (1979) used $m = 1.75 - 0.5i$.

The measured size distributions for the aerosols in Fig. 5 are shown in Fig. 6a along with the corresponding values of B_a and ω (Fig. 6a, b, c) plotted as functions of wavelength. The mass mean diameters, D_g , for these experimental samples range from $0.24 \mu\text{m}$ to $0.59 \mu\text{m}$. Figure 6d, e, f includes similar plots for eight log-normal distributions with mass mean diameters of 0.2 to $1.2 \mu\text{m}$ and σ_g values of 1.3 and 2.0 . These ranges bracket those generally observed for atmospheric EC and should be compared to those in Fig. 6a determined for the various measured size distributions. At $\lambda = 550 \text{ nm}$ the range of D_p presented in Fig. 6a results in theoretical values of B_a ranging from about 4.4 to $9.0 \text{ m}^2 \text{ g}^{-1}$. This particle size distribution difference can account for the different B_a values for M71 generated by the two different methods. Variability over visible wavelengths is shown in Fig. 6b using two different geometric standard deviations for each mass mode diameter (1.3 is typical of several distributions reported here and 2.0 is a value often mentioned for urban soot). A factor of two variability in B_a can be seen for a typical range of distributions over the wavelength range associated with many atmospheric measurements (500 – 650 nm).

The modeled values of B_a (Fig. 6b) and B_s (specific scattering, $\text{m}^2 \text{ g}^{-1}$, not shown) for the M71 size distributions are larger for the smaller particle sizes indicated in Fig. 5. Values of B_a obtained from each technique lie within the range of theoretical values after allowances for experimental uncertainty. The difference between measured values and theory is generally less than among the measured values. The single scatter albedo, ω , shows less dependence on particle size than either B_s or B_a , as these parameters both increase with decreasing particle size. For the M71 calibration the modeled value for ω is 0.47 compared to the measured value of 0.40 . This suggests either a systematic underestimate of b_s with the nephelometer, a systematic overestimate of b_a by all techniques, an inappropriate complex refractive index chosen for modeling M71, or a combination of the above. Since the nephelometer was used to measure the

relative constancy of aerosol optical properties a careful absolute calibration was not performed. Hence, we suspect the nephelometer data but cannot eliminate the other possibilities.

An ambient sample collected at the University of Washington campus (UW AMBI2 in Table 1) and one collected in a motor vehicle tunnel in central Seattle are included in Figs 5 and 6. These represent possible examples of urban aerosol containing soot from diffuse and near sources, respectively. The high modeled values of B_a for these samples seen in Fig. 6a reflect the smaller particle sizes for these ambient aerosols compared to the M71 as shown in Fig. 5. The value for the tunnel sample is highest, as expected for aerosol collected near its source, and would be expected to decrease during atmospheric aging of the aerosol. If the soot fractions of these two aerosols have a size distribution similar to that shown for the total and if their optical properties are close to those modeled here, then the modeled specific absorption of 9 – $10 \text{ m}^2 \text{ g}^{-1}$ at 550 nm (Fig. 6b) brackets the reference value of $9.68 \text{ m}^2 \text{ g}^{-1}$ mentioned earlier. We believe this degree of agreement is fortuitous and that ambient soot variability will result in values that show greater differences. However, the use of this value as a reference value for the evaluation of ambient data appears reasonable.

CONCLUSION

We have presented an intercomparison of several techniques used to measure light-absorbing properties of M71 particles having a known size distribution. A linear relationship between optically derived absorbing carbon mass and gravimetrically determined carbon mass was present with all techniques for an order of magnitude range of concentrations collected on the filters. Empirically determined specific absorption values were compared to theoretical estimates based upon measured properties of the M71 aerosol size distribution. These comparisons indicate that absorption measurements made by the integrating plate, integrating sphere and integrating sandwich methods generally show agreement within about 30%. The variation in specific absorption as a function of size expected from Mie theory was observed by all methods and quantitative agreement within about 20% was found.

Comparisons of the integrating plate method, with and without a neutral density filter (NDF), showed the former to give a positive bias to the absorption measurement as discussed elsewhere (Clarke, 1982; Weiss and Waggoner, 1984). Integrating plate values corrected according to the model of Clarke (1982a) were lower than both normal or NDF values and closest to theoretical values.

The use of $9.68 \text{ m}^2 \text{ g}^{-1}$ as a representative calibration value for specific absorption (at 550 nm) of

M71 appears reasonable provided M71 particle diameters are kept close to ambient values, $0.1 < D_p < 0.3 \mu\text{m}$. The lower values of B_a found by all techniques for the larger M71 test aerosol used here are consistent with the modeled value for these sizes. The measurement discrepancy seen among techniques presented here is about 10–30 % and probably smaller than the uncertainties associated with absorption measurements on ambient soot aerosol due to the natural variability in its size distribution and morphology. Moreover, the conversion of optical absorption data to soot concentrations and vice versa are likely to be uncertain by more than this amount for data typically obtained without detailed microphysical data on the soot size distribution. Consequently, a further improvement in the accuracy of measurement techniques may be of limited value. It is hoped that similar and more extensive intercomparisons of other techniques may allow greater comparison of diverse data sets by identifying any systematic differences among the methods.

Acknowledgements—We thank W. Wiscombe for use of his programs for Mie calculations. The computations were done at the National Center for Atmospheric Research. This work was partially supported by NSF grants ATM-82-15337, DPP-8442921 and EPA grant R812896-01-0. Hawaii Institute of Geophysics Contribution 1836.

REFERENCES

- Ball R. J. and Robinson G. D. (1982) The origin of haze in the Central United States and its effects on solar irradiation. *J. appl. Met.* **2**, 171–188.
- Bergstrom R. W. Jr. (1972) Predictions of the spectral absorption and extinction coefficients of an urban air pollution aerosol model. *Atmospheric Environment* **6**, 247–258.
- Bergstrom R. W. (1973) Extinction and absorption coefficients of the atmospheric aerosol as a function of particle size. *Beitrage zur Physik der Atmosphere*, 223–234.
- Charlson R. J. and Pilat M. J. (1969) Climate: the influence of aerosols. *J. appl. Met.* **8**, 1001.
- Clarke A. D. (1982a) Effects of internal reflection coefficient on light absorption measurements made using the integrating plate method. *Appl. Optics* **21**, 3021–3031.
- Clarke A. D. (1982b) Integrating sandwich: a new method of measurement of the light absorption coefficient for atmospheric particles. *Appl. Optics* **21**, 3011–3020.
- Clarke A. D., Charlson R. J. and Radke L. F. (1984) Airborne observations of Arctic aerosol—IV. Optical properties of Arctic haze. *Geophys. res. lett.* **11**, 405–408.
- Clarke A. D. and Noone K. J. (1985) Soot in the Arctic snowpack: a cause for perturbations in radiative transfer. *Atmospheric Environment* **12**, 2045–2053.
- Donoian H. C. and Medalia A. I. (1967) Scattering and absorption of light by carbon black. *J. Paint Technol.* **39**, 716–727.
- Fischer K. (1970) Bestimmung der Absorption von sichtbare Strahlung durch Aerosolpartikeln. *Contr. atmos. Phys.* **43**.
- Gerber H. and Hindman E. H. (eds) (1982) *Light Absorption by Aerosol Particles*. Spectrum Press, Hampton, VA.
- Heintzenberg J. (1982) Size segregated measurements of particulate elemental carbon and light absorption at remote Arctic locations. *Atmospheric Environment* **16**, 2461–2469.
- Jantzen J. (1979) Refractive index of colloidal carbon. *J. Colloidal Interface Sci.* **3**, 436–437.
- Kawa S. R. and Pearson R. (1984) Absorption of sunlight by aerosol as a heat source in the planetary boundary layer. Paper A31A-07, *EOS*, **65**, 838.
- Lin C. L., Baker M. B. and Charlson R. J. (1973) Absorption coefficient for atmospheric aerosols: a method for measurement. *Appl. Optics* **12**, 1356–1363.
- Mie G. (1908) Beitrage zur Optik truber Medien. *Ann. Phys.* **25**, 377–445.
- Pollack J. B. and Cuzzi J. N. (1980) Scattering by nonspherical particles of size comparable to a wavelength: a new semi-empirical theory and its application to tropospheric aerosols. *J. atmos. Sci.* **37**, 868–881.
- Roessler D. M. and Faxvog F. R. (1979) Optoacoustic measurement of optical absorption in acetylene smoke. *J. Opt. Soc. Am.* **69**, 1699–1704.
- Roessler D. M. and Faxvog F. R. (1980) Optical properties of agglomerated acetylene smoke particles at 0.5145 and 10.6 μm optical wavelengths. *J. Opt. Soc. Am.* **70**, 230–235.
- Senftleben H. and Benedict E. (1917) Uber die optischen Konstanten und die Strahlungsgesetze der Kohle. *Annalen der Physik* **359**, 65–68.
- Twitty J. T. and Weinman J. A. (1971) Radiative properties of carbonaceous aerosols. *J. appl. Met.* **8**, 725–731.
- Twomey S. and Hoffman D. R. (1982) Workshop Review. In *Light Absorption by Aerosol Particles* (edited by German H. and Hindman E.), pp. 398–408. Spectrum Press.
- Weiss R. E. and Waggoner A. P. (1982) *Particulate Carbon* (edited by Wolff G. T. and Klimsch R. L.). Plenum, New York.
- Weiss R. E. and Waggoner A. P. (1982) *Particulate Carbon* (edited by Wolff G. T. and Klimsch R. L.). Plenum.
- Weiss R. E. and Waggoner A. P. (1984) Aerosol optical absorption: accuracy of filter measurement by comparison with in-situ extinction. In *Aerosols* (edited by Liu, Pui and Frissan), pp. 397–400. Elsevier.
- Whitby K. T. (1979) Size distribution and physical properties of combustion aerosols. *Proc. Conf. on Carbonaceous Particles in the Atmosphere*, Lawrence Berkeley Laboratory, Berkeley, California. NTIS document LBL-9037.
- Wiscombe W. J. (1980) Improved Mie scattering algorithms. *Appl. Optics* **19**, 1505–1509.